# Spin-Polarized Electron Tunneling in bcc FeCo/MgO/FeCo(001) Magnetic Tunnel Junctions

F Bonell, Thomas Hauet, S Andrieu, F Bertran, P Le Fèvre, Lionel Calmels, A Tejeda, F Montaigne, Bénédicte Warot-Fonrose, B Belhadji, et al.

# Spin-Polarized Electron Tunneling in bcc FeCo/MgO/FeCo(001) Magnetic Tunnel Junctions

F. Bonell,[1] T. Hauet,[1] S. Andrieu,[1,*] F. Bertran,[2] P. Le Fèvre,[2] L. Calmels,[3] A. Tejeda,[1,2] F. Montaigne,[1] B. Warot-Fonrose,[3] B. Belhadji,[3] A. Nicolaou,[2] and A. Taleb-Ibrahimi[2]

[1]*Institut Jean Lamour, Nancy University-CNRS, Bd des Aiguillettes, BP239, 54506 Vandoeuvre-lès-Nancy, France*
[2]*Synchrotron SOLEIL-CNRS, L'Orme des Merisiers, Saint-Aubin, BP48, 91192 Gif-sur-Yvette cedex, France*
[3]*CEMES-CNRS, Université de Toulouse, 29 rue Jeanne Marvig, 31055 Toulouse, France*

(Received 20 December 2011; published 25 April 2012)

In combining spin- and symmetry-resolved photoemission, magnetotransport measurements and *ab initio* calculations we detangled the electronic states involved in the electronic transport in $Fe_{1-x}Co_x(001)/MgO/Fe_{1-x}Co_x(001)$ magnetic tunnel junctions. Contrary to previous theoretical predictions, we observe a large reduction in TMR (from 530 to 200% at 20 K) for Co content above 25 atomic % as well as anomalies in the conductance curves. We demonstrate that these unexpected behaviors originate from a minority spin state with $\Delta_1$ symmetry that exists below the Fermi level for high Co concentration. Using angle-resolved photoemission, this state is shown to be a two-dimensional state that occurs at both $Fe_{1-x}Co_x(001)$ free surface, and more importantly at the interface with MgO. The combination of this interface state with the peculiar density of empty states due to chemical disorder allows us to describe in details the complex conduction behavior in this system.

DOI: 10.1103/PhysRevLett.108.176602 PACS numbers: 72.25.−b, 73.40.Gk, 79.60.−i, 81.15.Hi

Since the discovery of giant magnetoresistance (GMR) in spin valves in 1988 [1], a new branch of physics referred to as spintronics has considerably developed. The discovery of the large tunnel magnetoresistance (TMR) in 1995 [2], the prediction of the spin-transfer mechanism in 1996 [3,4], and the demonstration of spin-dependent coherent tunneling in MgO-based epitaxial MTJs in 2001-2004 [5–10], have largely contributed to developments in this field. Currently, a number of new areas are being explored, such as rf oscillators, devices and memories based on the spin-transfer-torque effect, electric field assisted switching, magnonics, or spincaloritronics [11]. In addition, industrial-scale devices such as magnetic recording heads already use the exceptional electrical properties of GMR and TMR. The technology transfer from research to industry continues today, with MRAM demonstrators based on MgO-based MTJs [12] and rf oscillators using spintronics devices. While commercialization as well as broad utilization into various areas of research has been rapid for spintronic devices, in many cases a full understanding of the underlying physics is lacking. MgO-based MTJs with FeCo or FeCoB electrodes are a striking example of this situation.

FeCo(B)/MgO/FeCo(B)(001) multilayers, fabricated by molecular beam epitaxy (MBE) or sputtering deposition are widely utilized for their high spin current injection efficiency and exceptional electrical sensitivity to any change in the magnetic configuration of the electrodes. Because of the huge TMR predicted by *ab initio* calculation for the equimolar and $B2$ ordered $Fe_{0.5}Co_{0.5}$ alloy and for pure bcc Co (1000%–6000% at 0 K [13]), bcc FeCo(001) electrodes are now extensively used in MTJ fabrication. However, the situation is not so clear regarding the reported results. First, large TMR were actually obtained on MBE grown Fe/bcc Co/MgO/Co/Fe(001) [14]. However, a heating of the whole stacking up to 250 °C during 30 minutes suggest a possible alloying between Fe and Co. On the other hand, contrary to expectations, epitaxial $Fe_{0.5}Co_{0.5}$/MgO/Fe(001) and Fe/MgO/Fe(001) MTJs exhibit the same TMR [15]. It should be noted that the $B2$ order assumed in Ref. [13] is not observed. Finally, reported TMR of sputtered FeCo/MgO/FeCo(001) MTJs present a nonmonotonic dependence as a function of the Co concentration with a maximum around 25% of Co [16]. The detailed effect of Co alloying into Fe on the spin-dependent tunneling remains therefore obscure.

In this Letter, we explain quantitatively the unexpected transport properties observed in FeCo/MgO/FeCo(001) MTJs. We demonstrate that transport measurements alone are not sufficient to complete the current understanding of this system, and that spin-, symmetry-, and angle-resolved photoemission, together with DFT calculations taking into account the chemical disorder, offer a unique path to probing directly the tunneling electrons. We use a specific photoemission experiment to untangle the different Bloch waves responsible for the conduction along (001) as a function of their symmetry ($\Delta_1$ or $\Delta_5$) and spin state (majority $\uparrow$ or minority $\downarrow$), in contrast to standard transport measurements where all these contributions are mixed.

bcc MgO-based MTJs with $Fe_{1-x}Co_x(001)$ electrodes were grown by coevaporation using MBE. The epitaxial relationship, growth mode, and surface flatness were controlled using reflection high energy electron diffraction (RHEED). In addition, the evaporation rates of the Co and Fe sources, and consequently the alloys stoichiometry, were accurately controlled by recording the intensity

 

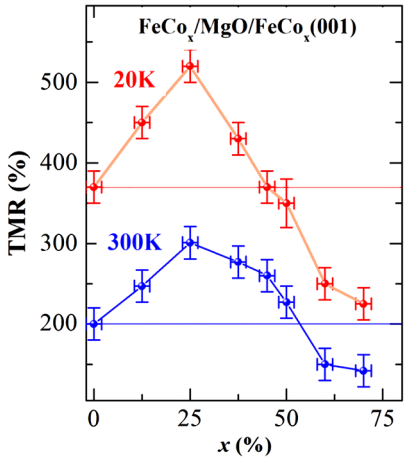


FIG. 1 (color online). TMR measured at 20 K and 300 K on a series of bcc $Fe_{1-x}Co_x$/MgO/$Fe_{1-x}Co_x$(001) MTJs grown by MBE.

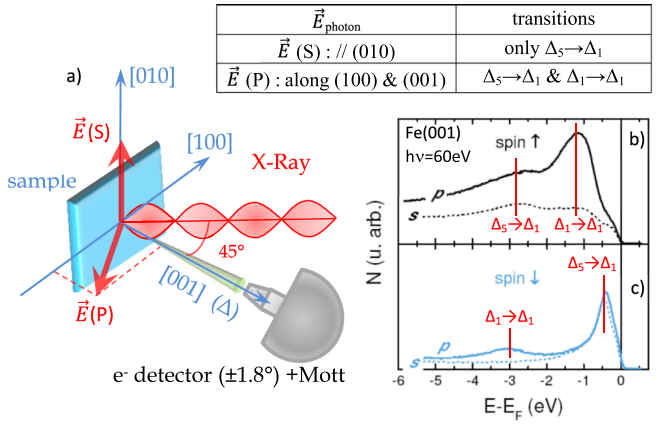


FIG. 2 (color online). (a) Schemes of the SR-PES experiment and measurement on Fe(001) for majority spins (b) and minority spins (c) The incident photon field is in-sample-plane for $s$ polarization and can be projected in sample in-plane and out-of-plane components for $p$ polarization. The small aperture of the detector allows detecting electrons only with $\Delta$ symmetry.

oscillations of the diffracted electron beam. Preserving the bcc structure is crucial to achieving the appropriate electronic band structure leading to large TMR. Using RHEED analysis, it was verified that the $Fe_{1-x}Co_x$ alloys retain the bcc structure found in pure Fe up to a Co concentration $x = 0.7$, but relaxes to the hcp structure for higher values of $x$. Accordingly, transport measurements were only performed on $Fe_{1-x}Co_x$(50 nm)/ MgO(2.5 nm)/ $Fe_{1-x}Co_x$(20 nm)/Co(30 nm)(001) MTJs with $0 \leq x \leq 0.7$. Micron-size MTJs were patterned by optical lithography and Ar ion milling. Figure 1 displays the TMR variations as a function of $x$, at 300 and 20 K. As expected theoretically, the TMR increases continuously from $x = 0$ to $x = 0.25$, but a dramatic decrease is observed for larger values of $x$. A similar behavior was previously reported for sputtered FeCoB/MgO/FeCoB MTJs [16], but the authors explained this anomaly by crystallization issues in their FeCoB alloys for high Co contents. Such reasoning, however, cannot be applied to the case of single-crystal samples like ours. Consequently, our results demonstrate that at a fundamental level, the optimum Co concentration to obtain the most sensitive TMR devices or the most highly polarized current injector based on FeCo(B)/MgO/FeCo(B) MTJs is around 25% of Co, and not 40–80% as overwhelmingly used in ongoing research and applications [17–20].

To understand this behavior, information on both *spin* and *symmetry* of tunneling electrons are needed. For that purpose, photoelectron spectroscopy (PES) experiments were conducted at the SOLEIL synchrotron radiation source, on the CASSIOPEE beam line [21]. Samples were grown *in situ*, in a MBE chamber coupled both to the spin-resolved (SRPES) and the angle-resolved photoemission (ARPES) experimental chambers. The geometry used in both experiments is shown in Fig. 2. The small aperture of the detector allows detecting electrons only with $\Delta$ symmetry. Moreover, the spin information is obtained in SRPES using a Mott detector added to the energy detector. Finally, the photon polarization is used. We used two experimental geometries [Fig. 2(a)] with the light polarization either out of the plane ($s$ polarization) or in the plane of incidence ($p$ polarization). The final states reached by photoemission are far above the Fermi level ($E_F$) and have the $\Delta_1$ symmetry of free electrons [22,23]. The dipolar selection rules indicate that only the initial states having the same symmetry as the electric field with respect to the [001] direction can be excited. Thus, in $s$ polarization, only $\Delta_5 \rightarrow \Delta_1$ transitions are explored, whereas both $\Delta_5 \rightarrow \Delta_1$ and $\Delta_1 \rightarrow \Delta_1$ transitions occur in $p$ polarization. An illustration of this orbital selectivity is given in Fig. 2(b) on Fe(001) at a photon energy of 60 eV. The peaks observed in PES spectra of (001) Fe film can be assigned unambiguously: when a transition is seen for both photon polarizations, the excited state's symmetry is $\Delta_5$, and when it is only seen using $p$ polarization, it is $\Delta_1$. The observed $s$ and $p$ peaks in Fig. 2 fit well with theoretical predictions [5] and previous experimental data. Using both photon polarizations sequentially allows us to determine the symmetry of the detected peaks in the photoemission spectra. Such unique information is crucial in correctly understanding which states may participate in the spin-polarized electrical transport in MTJs.

Spin-resolved photoemission spectra were recorded at $h\nu = 60$ eV for both $s$ and $p$ polarizations on different bcc $Fe_{1-x}Co_x$ films grown on Fe(001) buffer layers [Fig. 3(a)]. The alloy layer thickness chosen between 5 and 10 monolayers (ML) is small enough to keep the bcc structure in the whole $x$ range. The spectra were measured in normal emission ($\Delta$ direction). The observed peaks are assigned using the density of states (DOS) calculated from first principles for bulk bcc $Fe_{1-x}Co_x$ alloys as described in

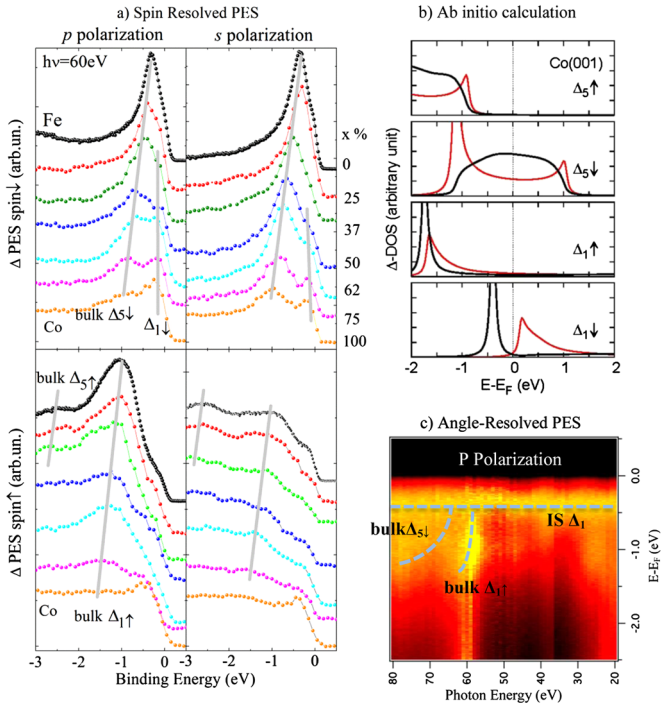


FIG. 3 (color online). (a) Spin-resolved PES spectra obtained at 60 eV photon energy on a series of $Fe_{1-x}Co_x$ (001) layers uncovered by MgO, $x$ varying from 0 to 100%. The gray lines are guide to the eyes to visualize the energy displacement of the peaks. (b) $\Delta_1$ and $\Delta_5$ DOS calculated from first principles for the free Co(001) surface (red: bulk DOS, dark: surface DOS). (c) ARPES measurement using $p$ polarization performed on bcc Co(001) film covered by MgO.

Ref. [24]. The substitutional atomic disorder between Fe and Co inside the bcc lattice was treated using the coherent potential approximation (CPA). Starting with the minority spin, as expected from the calculations [Fig. 3(b)], a clear signature of the $\Delta_5 \downarrow$ state is observed in the spectra for all concentrations [Fig. 3(a)-upper panel]. As the Co concentration is increased, $E_F$ is displaced in energy as the bands are filled, and the peaks are shifted towards higher binding energy. For $x$ up to 25%, the PES spectra using $s$ and $p$ polarizations are similar, meaning that there is no $\Delta_1 \downarrow$ state in this energy range. However, starting at $x = 37\%$ and continuing to pure Co, an additional minority spin peak is resolved around $-0.4$ eV below $E_F$, which is not predicted from the calculated bulk DOS. This peak is strongly attenuated in $s$ polarization, which means that the symmetry character of this state is $\Delta_1$. Next we look at the majority spin spectra [Fig. 3(a)—lower panel]. For $p$ polarization, the strong peak at $-1$ eV observed for pure Fe originates from the $\Delta_1 \uparrow$ band. As expected, the intensity of this peak is strongly decreased for $s$ polarization. Another contribution is observed around $-2.5$ eV for both polarizations which is consistent with the $\Delta_5 \uparrow$ band. The different transitions observed by PES are therefore all consistent with the calculated density of bulk states, except a new $\Delta_1 \downarrow$ state observed close to the Fermi level at Co concentrations of 37% or more.

What is the nature of this new $\Delta_1 \downarrow$ state? It is well known that a $\Delta_1$ surface state exists at bcc (001) free surfaces. An empty surface state has been indeed identified on Fe(001) [25–27]. *Ab initio* calculations show that it is still present at the Fe/MgO interface as an interfacial state (IS) coupled to bulk propagating states and thus named interface resonant state (IRS) [5,27]. However, no direct experimental evidence of the IS and of its influence on transport in CoFe/MgO-based MTJs had been provided up to now. As the incorporation of Co electrons dopes the material with electrons, the IS should be gradually filled in FeCo alloys. *Ab initio* calculations confirm that this surface state is actually below $E_F$ for the bcc Co(001) free surface [Fig. 3(b)]. Therefore, it should appear as a growing peak close to $E_F$ in the PES spectra, in accordance with our observations. Photoemission also shows that this state is clearly below $E_F$ for $x > 50\%$. However, a small spectral weight is also observed between 37% and 50% Co. Since this state is empty for pure Fe, this means that it crosses $E_F$ with increasing Co content. To further confirm its 2D nature, we performed ARPES measurements to examine the dispersion along $\Delta$. For a 2D state, no dispersion is expected perpendicularly to the surface because, contrary to a bulk state, its binding energy should remain constant with $k_\perp$ (the wave vector's component perpendicular to the surface, so along $\Delta$). Furthermore, our ARPES measurements were performed on a MgO-coated film, to confirm that the surface state still exists at the interface with MgO. This verification is critical to verify that the IS will be relevant in the transport process in a MTJ. The ARPES experiments were conducted on a 5 ML pure bcc Co film covered by 1.2 ML of MgO. The photon energy was varied from 20 to 80 eV in order to scan $k_\perp$ over a whole Brillouin zone. As previously, the electrons were collected along the $\Delta$ direction. The obtained maps do not give a direct picture of the band structure, since the relationship between the photon energy and $k_\perp$ is not linear and the intensity of the spectra is perturbed by the MgO contribution [28,29]. We know however that photons with energy above 60 eV probe the bands near the $\Gamma$ point [29], and the bcc Co bulk bands are known. As for spin-resolved experiments, the polarization dependence of the spectra allowed us to unambiguously identify the $\Delta_1 \uparrow$ and $\Delta_5 \downarrow$ bulk bands. The results (binding energy versus photon energy) are shown for $p$ polarization [Fig. 3(c)]. The new $\Delta_1 \downarrow$ state discussed before is clearly observed at a constant binding energy, and is thus a two-dimensional (2D) state. For $s$ polarization (not shown), we actually observed that this IS is strongly attenuated in the whole photon energy range, confirming its $\Delta_1$ symmetry. To summarize, four important results are obtained from our combined spin-resolved PES and ARPES analysis: First, this new state has a 2D character. Second, this state is an interface state since it is still

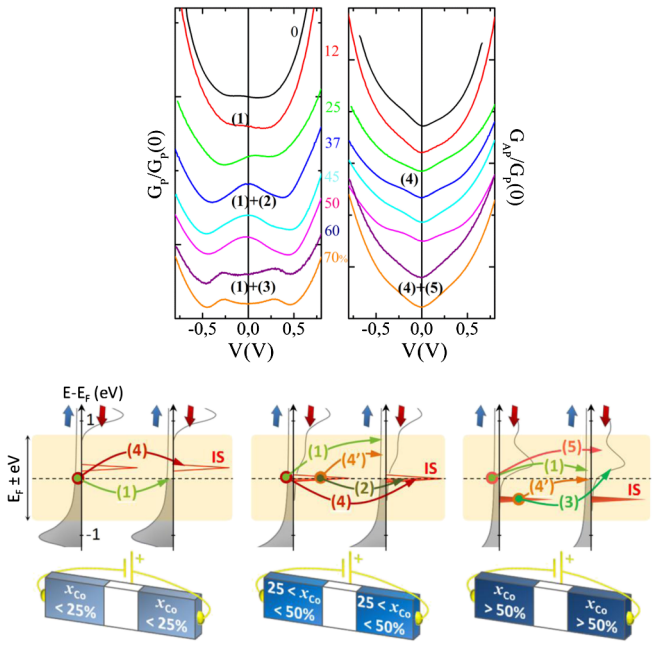


FIG. 4 (color online). *Top*, parallel $G_P(V)$ and antiparallel $G_{AP}(V)$ conductances of samples in Fig. 1, and *bottom,* possible conduction channels with $\Delta_1$ symmetry (see text).

clearly visible on a MgO-coated film. Third, the symmetry of this state is $\Delta_1 \downarrow$. And fourth, this interface state which is empty for pure Fe, starts crossing $E_F$ at least above 25% Co, and is fully occupied above 50% Co.

Based on our PES results, we can now go further in understanding the transport, and especially the conductance curves reported in Fig. 4. During the tunneling process in such epitaxial systems, the electron symmetry and spin are conserved (coherent tunneling); the current is essentially driven by $\Delta_1$ symmetry states, the barrier attenuation being much stronger for the other symmetries [5,6]. Finally, conduction is explained by tunneling from an occupied band of the first electrode to an unoccupied band of the second electrode. Thus, the transport in parallel ($P$) configuration consists of two contributions from the $\Delta_1 \uparrow$ occupied states to the $\Delta_1 \uparrow$ empty states and from $\Delta_1 \downarrow$ occupied states to $\Delta_1 \downarrow$ empty states. On the other hand, transport in the antiparallel ($AP$) configuration includes two components, from $\Delta_1 \uparrow$ occupied states to $\Delta_1 \downarrow$ empty states and vice versa. A general overview of the different conduction channels discussed in detail below is given in Fig. 4.

If we consider only the bulk bands of pure bcc Fe, $\Delta_1 \downarrow$ states are far from $E_F$ and therefore do not play any role in the conduction process when the voltage bias is lower than 1 V. Hence, there should be a unique conduction channel in $P$ configuration, from $\Delta_1 \uparrow$ to $\Delta_1 \uparrow$ (named channel 1 in Fig. 4), and no conduction in $AP$ configuration, giving an infinite TMR. Limited TMR are however observed due to the occurrence of non-$\Delta$ (states with in-plane component $k_{\parallel} \neq 0$) and $\Delta_5$ channels in $AP$ conductance. Adding the minority spin IS discussed above for pure Fe, calculations show that it is empty [25,27], thus providing a $\Delta_1 \uparrow \rightarrow \Delta_1 \downarrow$ conduction channel in the $AP$ configuration (channel 4) [30,31].

According to our PES data, this description remains valid up to around $x = 37\%$. For Co contents from 37% to 50%, the IS becomes partially filled, which opens new conduction channels in both $P$ and $AP$ configurations. In the $P$ configuration, the $\Delta_1$(IS) $\downarrow \rightarrow \Delta_1$(IS) $\downarrow$ channel (channel 2) explains the small bump observed around 0 V in $G_P(V)$, which appears in a small voltage range since the IS has a small energy width. Note that this bump is observed in $G_P(V)$ even down to $x = 25\%$, although the IS was not clearly detected by PES for this Co content. In the $AP$ configuration, the consequences for the voltage dependence are much less dramatic. Indeed, the new $\Delta_1$(IS) $\downarrow \rightarrow \Delta_1$(Bulk) $\uparrow$ transport channel (channel 4') is towards bulk $\Delta_1 \uparrow$ empty states, the density of which is almost constant in energy. Hence, the $\Delta_1$(IS) $\downarrow \rightarrow \Delta_1$(Bulk) $\uparrow$ conduction channel can occur at any voltage and does not show up as a distinctive structure in the conductance curves.

For $x > 50\%$, the IS is completely filled, which closes all the conduction channels towards empty $\Delta_1$(IS) $\downarrow$ states. However, *ab initio* calculations including Fe/Co chemical disorder (not taken into account in Ref. [13]) show that bulk $\Delta_1 \downarrow$ empty states are now very close to $E_F$ [24], providing efficient conduction channels in each configuration. Indeed, for conductance curves in the $P$ configuration, the structures between $-0.5$ and $+0.5$ V are due to the $\Delta_1$(IS) $\downarrow \rightarrow \Delta_1$(Bulk) $\downarrow$ channel (channel 3), and can be seen as the convolution of the IS (close to a Dirac function) and the empty bulk $\Delta_1 \downarrow$ DOS, which presents a clear peak around 0.1 eV [see Fig. 3(b) and [24]]. In the $AP$ configuration, a $\Delta_1$(Bulk) $\uparrow \rightarrow \Delta_1$(Bulk) $\downarrow$ channel (channel 5) may now be activated, leading to a large increase of $G_{AP}(V)$ conductance above around 0.5 V. This increase is strong enough to reverse the sign of the TMR above 0.7 V.

To summarize, the TMR decrease is naturally explained by the vanishing of the $\Delta_1$ half-metallic behavior for Co contents larger than 25%, originating from the occurrence of $\Delta_1$(IS) $\downarrow$ and by the existence of empty $\Delta_1$(bulk) $\downarrow$ just above $E_F$.

In conclusion, our spin- and symmetry-resolved photoemission experiments coupled to transport measurements and *ab initio* calculations hence give a complete description of tunneling transport in FeCo/MgO(001) based tunnel junctions, including TMR and conductance anomalies. These experiments highlight the existence of a 2D electronic state, confined at the interface between the magnetic layer and the MgO tunnel barrier. To our knowledge, it is the first experimental evidence of this interface state, so far only suspected to exist at the Fe/MgO interface. In addition, the chemical disorder in the bcc lattice leads to an empty $\Delta_1$(bulk) $\downarrow$ band very close to $E_F$ and strongly affects the TMR. This global approach,

combining macroscopic transport measurements together with deep insight into the fine electronic structure using both photoemission through an MgO overlayer and *ab initio* calculations, opens wide prospects for a more complete understanding of the coherent spin-polarized electron transport in magnetic tunnel junctions.

*Corresponding author.


[1] M. N. Baibich, J. M. Broto, A. Fert, F. Nguyen Van Dau, F. Petroff, P. Etienne, G. Creuzet, A. Friederich, and J. Chazelas, Phys. Rev. Lett. **61**, 2472 (1988).

[2] J. S. Moodera, L. R. Kinder, T. M. Wong, and R. Meservey, Phys. Rev. Lett. **74**, 3273 (1995).

[3] J. C. Slonczewski, J. Magn. Magn. Mater. **159**, L1 (1996).

[4] L. Berger, Phys. Rev. B **54**, 9353 (1996).

[5] W. H. Butler, X. G. Zhang, T. C. Schulthess and J. M. MacLaren, Phys. Rev. B **63**, 054416 (2001).

[6] J. Mathon and A. Umerski, Phys. Rev. B **63**, 220403 (2001)

[7] M. Bowen, V. Cros, F. Petroff, A. Fert, C. MartínezBoubeta, J. L. Costa-Krämer, J. V. Anguita, A. Cebollada, F. Briones, J. M. de Teresa, L. Morellón, M. R. Ibarra, F. Güell, F. Peiró, and A. Cornet, Appl. Phys. Lett. **79**, 1655 (2001).

[8] J. Faure-Vincent, C. Tiusan, E. Jouguelet, F. Canet, M. Sajieddine, C. Bellouard, E. Popova, M. Hehn, F. Montaigne, and A. Schuhl, Appl. Phys. Lett. **82**, 4507 (2003).

[9] S. Yuasa, T. Nagahama, A. Fukushima, Y. Suzuki, and K. Ando, Nature Mater. **3**, 868 (2004).

[10] S. S. P. Parkin, C. Kaiser, A. Panchula, P. M. Rice, B. Hughes, M. Samant and S. H. Yan, Nature Mater. **3**, 862 (2004).

[11] A. Fert, Rev. Mod. Phys. **80**, 1517 (2008).

[12] C. Chappert, A. Fert, and F. N. V. Dau, Nature Mater. **6**, 813 (2007).

[13] X. G. Zhang and W. H. Butler, Phys. Rev. B **70**, 172407 (2004).

[14] S. Yuasa, A. Fukushima, H. Kubota, Y. Suzuki, and K. Ando, Appl. Phys. Lett. **89**, 042505 (2006).

[15] S. Yuasa, T. Katayama, T. Nagahama, A. Fukushima, H. Kubota, Y. Suzuki, and K. Ando, Appl. Phys. Lett. **87**, 222508 (2005).

[16] Y. M. Lee, J. Hayakawa, S. Ikeda, F. Matsukura, and H. Ohno, Appl. Phys. Lett. **90**, 212507 (2007).

[17] J. C. Sankey, Y-T. Cui, J. Z. Sun, J. C. Slonczewski, R. A. Buhrman, and D. C. Ralph, Nature Phys. **4**, 67 (2007).

[18] S-C. Oh, S-Y Park, A. Manchon, M. Chshiev, J-H Han, H-W. Lee, J-E. Lee, K-T. Nam, Y. Jo, Y-C. Kong, B. Dieny, and K-J. Lee, Nature Phys. **5**, 898 (2009).

[19] A. Chanthbouala, R. Matsumoto, J. Grollier, V. Cros, A. Anane, A. Fert, A. V. Khvalkovskiy, K. A. Zvezdin, K. Nishimura, Y. Nagamine, H. Maehara, K. Tsunekawa, A. Fukushimà, and S. Yuasa, Nature Phys. **7**, 626 (2011).

[20] S. Ikeda, K. Miura, H. Yamamoto, K. Mizunuma, H. D. Gan, M. Endo, S. Kanai, J. Hayakawa, F. Matsukura, and H. Ohno, Nature Mater. **9**, 721 (2010).

[21] see for details http://www.synchrotron-soleil.fr/Recherche/LignesLumiere/CASSIOPEE.

[22] P. D. Johnson, Rep. Prog. Phys. **60**, 1217 (1997).

[23] L. N. Tong, F. Matthes, M. Muller, C. M. Schneider, and C. G. Lee, Phys. Rev. B **77**, 064421 (2008).

[24] B. Belhadji and L. Calmels, Phys. Rev. B **83**, 092401 (2011).

[25] J. A. Stroscio, D. T. Pierce, A. Davies, R. J. Celotta, and M. Weinert, Phys. Rev. Lett. **75**, 2960 (1995).

[26] M. M. J. Bischoff, T. K. Yamada, C. M. Fang, R. A. de Groot, and H. van Kempen, Phys. Rev. B **68**, 045422 (2003).

[27] L. Plucinski, Yuan Zhao, C. M. Schneider, B. Sinkovic, and E. Vescovo, Phys. Rev. B **80**, 184430 (2009).

[28] M. Sicot, S. Andrieu, P. Turban, Y. Fagot-Revurat, H. Cercellier, A. Tagliaferri, C. De Nadai, N. B. Brookes, F. Bertran, and F. Fortuna, Phys. Rev. B **68**, 184406 (2003).

[29] L. N. Tong, C. L. Deng, F. Matthes, M. Muller, C. M. Schneider, and C. G. Lee, Phys. Rev. B **73**, 214401 (2006).

[30] K. D. Belashchenko, J. Velev, and E. Y. Tsymbal, Phys. Rev. B **72**, 140404 (2005).

[31] C. Tiusan, M. Sicot, J. Faure-Vincent, M. Hehn, C. Bellouard, F. Montaigne, S. Andrieu, and A. Schuhl, J. Phys. Condens. Matter **18**, 941 (2006).